AES and EELS

Guido Falk von Rudorff

I Introduction

I.A Auger Electron Spectroscopy

In order to analyze the surface of a given sample, the Auger process might be used. It requires one core shell electron to be brought to a higher energy level, thus leaving a hole in the K-shell. Besides the usual relaxation by emission of photons, the energy can be transferred onto another electron from the atom. This electron leaves the atom shell and is called Auger electron.[1] As the energy differences between the three levels involved are material dependent, this method can be used in order to obtain information on the surface atoms' species together with their oxidation state[1]. For the oxidation and binding type, a rather high peak resolution of about 3 eV is necessary in order to tell the peaks apart. Oxidation in general causes a shift of about 10 eV—see Figure 2.

Although the Auger process itself is not limited to special shells, the KLL transition is the most frequent one for aluminium. The abbreviation KLL stands for the process letting one K shell electron ($n = 0, l = 0$) leave the core and one L electron ($n = 1, l = l_1$) replacing the K electron and one L electron ($n = 1, l = l_2$) replacing the other L electron. There are no restrictions on l_1 or l_2—not even on the ordering of the two numbers as the energy difference between the L shell and the K shell is much larger than the splitting of the L shell levels. However, the notation stays the same as the energies of the leaving electrons are the same, as well.

Regarding the K and L shells, this should lead to six transitions—all valid combinations of KL_iL_j with $i \leq j$. Experiments show three additional transitions due to the different coupling mechanisms. For small atomic numbers Z, the LS coupling is active and for large Z jj coupling becomes dominant. As the degeneracy of the transitions with respect to the final electronic states of the atom varies depending on the effective coupling, transitions for all nine final levels are detectable for atoms with intermediate Z. The actual transitions and their ordering for $Z < 50$ are given in Table I.

In case the main quantum number of all three electrons is the same, the transition is called a Coster-Kronig transition[1]. As the transition time is about 10^{-16} s, the broadening of these transitions is much larger than the usual broadening for KLL transitions[2] whose lifetime is about 10^{-15} s[1]. For both transition types, the broadening is caused by the uncertainty principle.

Usually, the Auger effect only affects the valence electrons. Therefore, the electron configuration of the elements relevant to this experiment are of particular interest—see Table II.

The measured electron energies are influenced by the work function E_W of the analyzer. Figure 1 shows the relevant information. In order to equilibrate the Fermi levels, both the sample and the analyzer are grounded. Therefore, the work function of the sample is irrelevant for the analysis. The resulting electron has the energy[4]

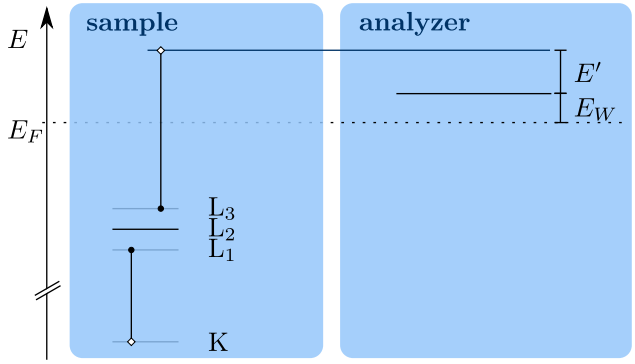

Figure 1. Schematic energy levels for a KL_1L_3 transition with the measured energy E' and the work function E_W.[1, 2]

$$E_e = E_i - E_k - E_j - E_W \tag{1}$$

where $E_i < E_k < E_j$ are the energies of the three energy levels involved. Unfortunately, these energy levels are subject to change after the first electron transition, as the shielding of the core of the atom gets less effective. For KLL transitions, the energy deviation can be estimated by raising the core charge by $\frac{\Delta Z}{e} \in [0.5, 1]$[1].

In order to determine the position of even very small peaks in the spectrum, usually the differentiated spectrum is plotted over the energy. Although the peaks' maxima are located at the zero crossing of the differentiated spectrum, the minimum of the high energy wing is

Table I. Energy ordering and electronic states for all possible KLL transitions[1]. Higher energy levels are listed first.

Label	Final State	Configuration
KL_3L_3	$^3P_2$	s^2 ↑↓ p^4 ↑ ↑ ↑↓
KL_3L_3	$^3P_0$	s^2 ↑↓ p^4 ↑↓ ↑ ↑
KL_2L_3	$^1D_2$	s^2 ↑↓ p^4 ↑↓ ↑↓
KL_1L_3	$^1S_0$	s^2 ↑↓ p^4 ↑↓ ↑↓ ↑↓
KL_1L_3	$^3P_2$	s^1 ↑ p^5 ↑ ↑↓ ↑↓
KL_2L_2	$^3P_1$	s^1 ↑ p^5 ↑ ↑↓ ↑↓
KL_1L_2	$^3P_0$	s^1 ↑ p^5 ↑ ↑↓ ↑↓
KL_1L_2	$^1P_1$	s^1 ↑ p^5 ↓ ↑↓ ↑↓
KL_1L_1	$^1S_0$	s^0 p^6 ↑↓ ↑↓ ↑↓

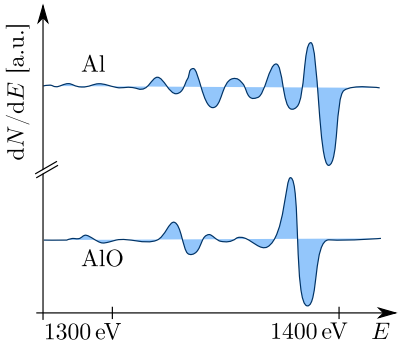

Figure 2. Section of a differentiated spectrum for aluminium and aluminium oxide.[5]

considered to be the peak position[1]. This corresponds to the high energy turning point of the peak. For multiple overlapping peaks, the differentiated spectrum is difficult to analyze and should be only considered together with the normal spectrum[1].

Chemical shifts and various loss mechanisms like plasmons can shift the peaks from the expected positions by several eV[1]. As the usual resolution is somewhat limited, the shifts are mainly observed as a general peak broadening. The peak width may depend on the energy of the primary electrons[1].

I.B Electron Energy Loss Spectroscopy

According to [1], there are five main groups of energy losses visible in the spectra. Electrons may get detached from the atom core by incident electrons, thus leaving ionized atoms. The peaks resulting from the scattered primary electrons are at a fixed position relative to the primary electron peak, the energetic distance of which is exactly the ionization energy. Obviously, the detached electrons are to be found at a fixed position in the spectrum, their ionization energy. Therefore, two peaks should be observed in case this effect plays an important role in the experiment. Nevertheless, the two peaks relative intensity in the measured spectra may vary due to the different angular distribution. The ionization energies are listed in Table III.

Besides this effect, electron excitations may be caused by the incident electron beam. These excitations may both include (interband) or exclude (intraband) transitions which require changing the main quantum number. Approximating the atoms by assuming them to be hydrogen-like, the energy differences for interband transitions may be estimated by

$$E = -\frac{Z^2}{n^2}E_r \Rightarrow \Delta E_{12} = Z^2\left(1-\frac{1}{4}\right)E_R \qquad (2)$$

which leads to ΔE_{12} of about 360 eV for interband and 20 eV for intraband transitions[1].

The particles of the third effect, the plasmons, are quasi particles describing oscillations of the valence electrons. Oscillation in this case means a collective weaving around the (approximately immovable) atom cores. The frequency and therefore the energy for a plasmon is given by

$$\omega_p = \frac{2e}{m}\sqrt{\pi\rho} \qquad (3)$$

where ρ is the valence electron density. In general, there are two possible plasmon types: the surface plasmons with a wavevector in the surface plane and the bulk plasmons with a wavevector perpendicular to the surface. For the surface plasmons, the frequency is given by

$$\omega_s = \frac{\omega_p}{\sqrt{1+\varepsilon}} \qquad (4)$$

where ε is the dielectric constant of the volume next to the surface not containing the surface itself. Both equations are based on the approximation of a free electron gas. These estimate values hold for aluminium[1]. Plasmon losses are in the order of 5 to 30 eV.

Both of the remaining two effects, the extended loss fine structure and the vibrational excitations should not be observable in this experiment as for the former the incident energy is too high and for the latter the energy loss is about 0.1 eV.

The bremsstrahlung background may be discriminated by using a highly monochromatic electron beam[6]. As each of the secondary electrons itself may be part of processes leading to tertiary electrons, the spectra suffer from a significant background noise that is difficult to describe. So far, there are two models: the Shirley and Tougaard one[6]. Both of them are suffering from unclear definitions[6].

The reference data for the four relevant spectra is given in Figure 3. In order to distinguish surface and bulk plasmons, usually the incident electron beam's angle would

Table II. Electron configurations and principal Auger lines[3] for all elements with atomic number Z relevant to this experiment.

Element	Z	Configuration	Auger Lines [eV]
Carbon	6	[He] $2s^2\ 2p^2$	
Oxygen	8	[He] $2s^2\ 2p^4$	510
Aluminium	13	[Ne] $3s^2\ 3p^1$	1350, 1400
Copper	29	[Ar] $3d^{10}4s^1$	650, 710, 790

Table III. First and second ionization energies in molar eV for elements relevant to this experiment.

Element	First Ionization	Second Ionization
Carbon	11.3	24.4
Oxygen	13.6	35.1
Aluminium	6.0	18.8
Copper	7.7	20.3

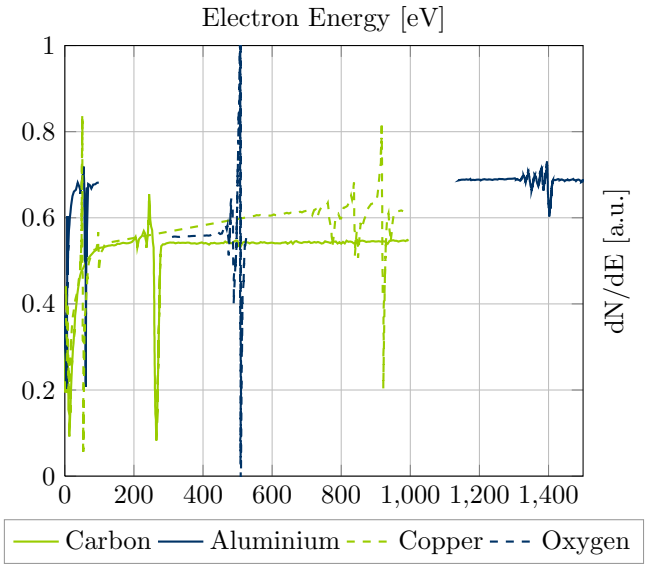

Figure 3. Auger spectra[3] for the elements relevant to this experiment. The relative peak intensity is conserved although the y axis is in arbitrary units.

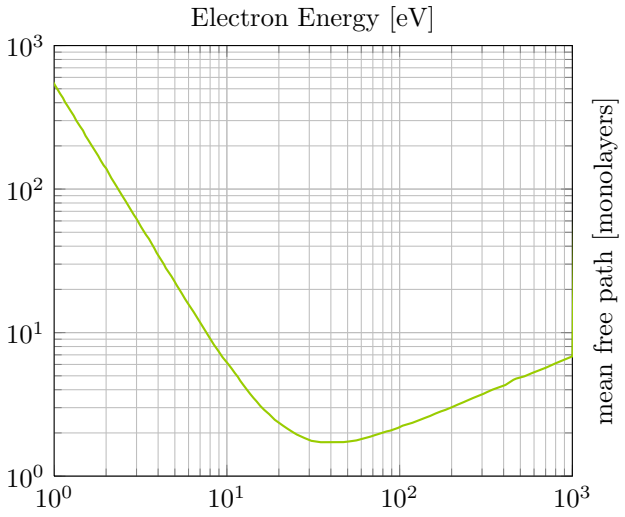

Figure 4. Mean free path for electrons depending on their kinetic energy[1].

be altered[1]. As for this experiment, this is impossible. Therefore, the kinetic energy of the electrons from the incident beam is varied so that the interaction of the primary electrons and the sample is either in the surface area or in the bulk part. However, one has to keep in mind that the signal cannot be separated clearly. Therefore, for different incident energies, both the peaks for surface and for bulk plasmons are expected. Only the relative intensity should vary under variation of the incident electrons' energy. Approximating the sample as a free electron gas and applying the Drude model, Figure 4 shows the mean free path of electrons in the sample. Besides the coarse dependency, the exact value is highly influenced by the material being observed[7].

I.C Cylindrical Mirror Analyzer

The cylindrical mirror analyzer got its name from two components of the setup. On the one hand, the sample itself is used as a mirror. For this experiment, the incident electron beam hits the target under an angle of 90 degrees. In general, different indicent angles are possible[1]. On the other hand, the analyzer allows for selecting a specific energy range for the count rate. This is done by two coaxial cylinders with a potential difference. Two circular slits allow both the secondary electrons and the deflected incident electrons to leave the inner cylinder. As the electric field between the cylinders deflects the electrons back to the inner cylinder again, the second slit selects those electrons that match a defined energy. The relative resolution $\Delta E/E$ is constant[1]. Thus, a higher energy leads to a higher absolute energy tolerance. Although this experiment only makes use of electrostatic effects, in general the Lorentz force may be used, as well. The electrons passing through the second slit, reach a photomultiplier. For the interpretation of the relative peak intensities, one has to keep in mind, that the gain function of the electron multiplier is not constant over the whole energy range and especially decreasing for less than 200 eV[3].

The cylindrical mirror analyzer has a quite good resolution, given that the primary electron beam is constant and nearly monoenergetic[1]. In order to reduce the noise, the electron beam should be focused as much as possible. Otherwise, the energy selection by the cylindrical mirror analyzer gets flawed.

The general energy error is given by[6]

$$\Delta E = \sqrt{\Delta E_e^2 + \Delta E_C^2 + \Delta E_L^2} \tag{5}$$

where ΔE_e is the beam energy width and ΔE_C denotes the passing energy window of the CMA, both adjustable properties of the experimental setup. The third parameter, the linewidth depends on the lifetime of the atomic states involved and is immutable.

II Setup

Using the file as intended was a quite tedious and less efficient method to reduce the contamination of the sample surface. One reason might be the age of the file, as due to the frequent use, the surface persumably got rather flat. However, the file cannot be rotated far enough in the vacuum chamber, so we were unable to actually look at the relevant side of the file. In order to overcome the less efficient method, we tilted the file a bit and used the edge of the file to scratch over the sample's surface over and over again. This method leads to far better results as shown in Figure 8.

The pressure was kept at about $3.2 \cdot 10^{-8}$ Torr. This value remained merley constant, even when using the file.

For the Auger spectrum and the bulk measurement, the oscillator level of the lock-in amplifier was set to 1.5. For the surface plasmon measurement, we used a value of 0.2.

The cleaning process was repeated after the intermediate lunch break.

III Spectra

III.A Uncleaned Sample

In the beginning, the Auger spectrum of the contaminated aluminium sample was analyzed. As the kinetic energy of the incident electrons was set to 4.8 keV for this part of the experiment, in theory the spectrum up to 4.8 keV should be measured. However, the experiment documentation imposes an experimental limit of 3 keV. Due to this restriction, we only sampled the energy range up to this energy. The relevant peaks from different materials are expected to be found within this range[3] (see Table II). This assumption holds for the KLL peaks, as well[8]. The overview spectrum in Figure 5 was recorded with a rasterization resolution of 1 eV. There was nearly no difference when compared to the averaged differential spectrum for three consecutive measurements.

Table IV presents the peaks found within the uncleaned spectrum. There are three main results. Firstly, no copper was found. As the vacuum chamber contains a copper sample, we expected to find some peaks related to this sample. The Auger peak of copper at 60 eV might be covered from the predominant aluminium peak at 68 eV, but at least the 920 eV peak of copper should be clearly identifiable. Secondly, we found a clear peak from sulfur. This is most interesting and yet difficult to explain. As normal air does not contain any significant amount of sulfur, the peak is unlikely to be caused by any influence from outside the chamber. As no sulfur sample is present, the sulfur peak has to be caused by outgassing. As the vacuum chamber is built for this exact purpose, we suppose the steel of which it is made to be sulfur free. This reasoning does not hold for the file, the spring and the sample holder. Either of which may be the reason for the sulfur trace. According to [3], the sulfur peak is very strong. Therefore, even a small concentration is assumed to lead to a visible peak. Some very often used types of steel contain up to 0.3% of sulfur[9]. Finally, we observed an offset of the energy scale. The offset is slowly raising with higher energies. It cannot be explained by the different notions of peak positions (estimated zero crossing of the differential spectrum versus minimal slope of the integrated spectrum), because we used the same method as the reference[3]. This offset is analyzed in detail in the discussion.

Table IV. Measured peaks from the uncleaned spectrum in Figure 5 using the very same labeling together with the theoretical values[3]. All values in eV.

Peak	Measured	Theoretical	Difference
$C^{(1)}$	16 ± 1	20 ± 1	4 ± 2
$Al^{(1)}$	72 ± 1	68 ± 1	4 ± 2
$S^{(1)}$	156 ± 1	152 ± 1	4 ± 2
$C^{(2)}$	279 ± 1	272 ± 1	7 ± 2
$N^{(1)}$	390 ± 1	381 ± 1	9 ± 2
$O^{(1)}$	483 ± 1	475 ± 1	8 ± 2
$O^{(2)}$	500 ± 1	490 ± 1	10 ± 2
$O^{(3)}$	521 ± 1	510 ± 1	11 ± 2
$Al^{(2)}$	1418 ± 1	1396 ± 1	22 ± 2

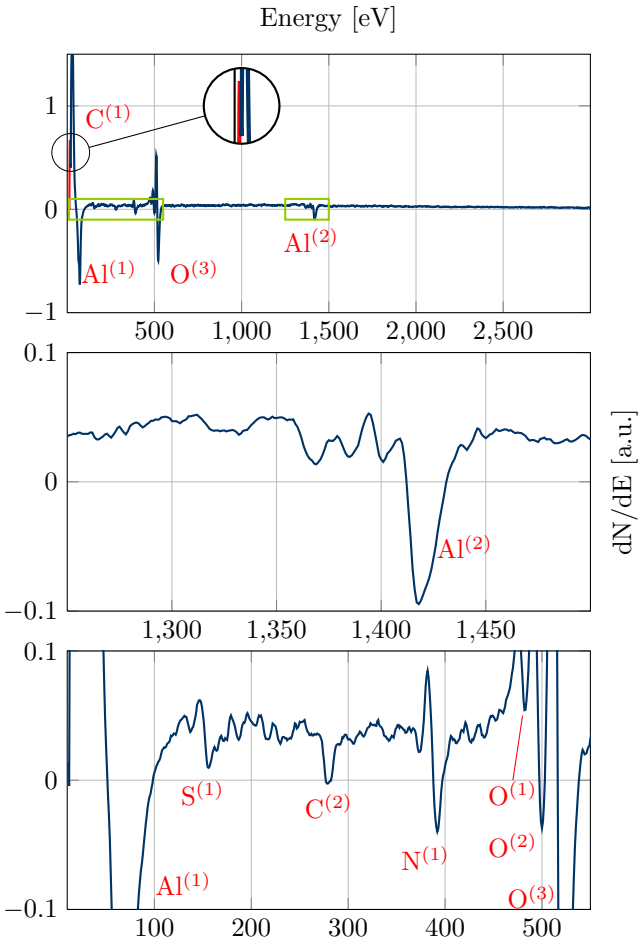

Figure 5. Measured Auger spectrum for the uncleaned sample (top) and two segments of the same spectrum (middle, bottom). The segments are highlighted with a green frame within the topmost diagram. The peak assignments are given in red. The energy scale is the one given by the experimental setup and does not match exactly the real peak positions—see text. The peak positions are listed in Table IV.

The success of the subsequent cleaning procedure was monitored by frequent overview spectra. Before starting this procedure which implied turning off the channeltron and the electron gun, we rotated the sample by about 10 degrees in order to check whether the surface angle has any visible impact on the resulting spectra. As the aluminium sample is curved instead of having a plain sur-

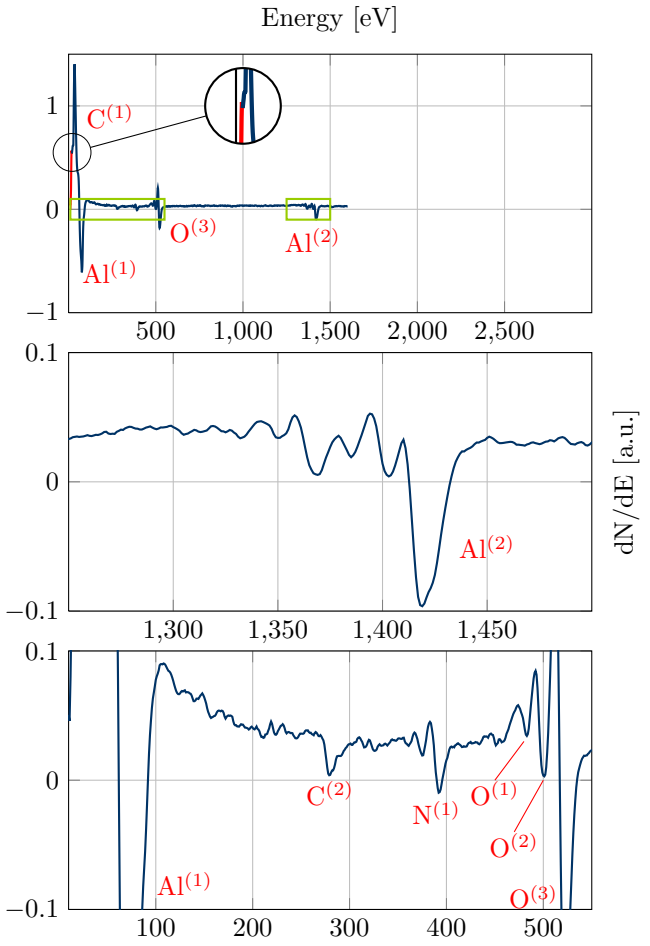

Figure 6. Measured Auger spectrum for the cleaned sample (top) and two segments of the same spectrum (middle, bottom). The segments are marked green within the topmost diagram. The peak assignments are given in red. The energy scale is the one given by the experimental setup and does not match exactly the real peak positions. The topmost frame uses the same scaling as Figure 5 to allow for easier comparison. No data for the rest of the spectrum has been recorded. The peak $C^{(1)}$ is very vague, yet detectable.

face, the impact angle is expected to change, as well. In theory, different incident angles should lead to different spectra[1]. However, depending on the surface roughness and the curvature, this effect should be small. In this experiment, we observed nearly no differences, as shown in Figure 7. Neither the peak to peak heights nor the peak positions seem to be influenced even for the moderate large rotation. Thus, we neglected the effect of different sample rotations for the rest of the experiment. However, we used the scale on the rotational axis to ensure that the same sample position up to an error of some two degrees was used. This is merely useful for the monitoring of the cleaning process.

The different peak heights for the oxygen and the aluminium peak in Figure 7 contain the information on relative surface coverage[1]. However, when interpreting the

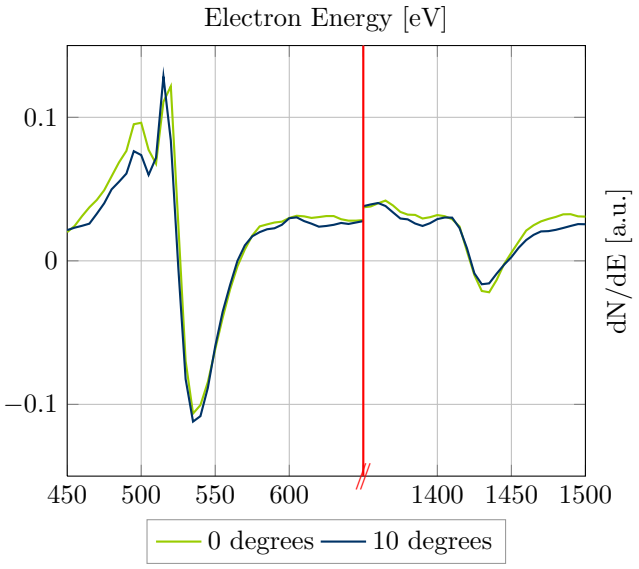

Figure 7. Measured Auger spectrum for the uncleaned sample for different rotations from the initial position. The red line denotes a discontinuity, as the spectrum in-between is of lesser interest. The left peak is due to the oxygen contamination, the right peak is resulting from the aluminium sample.

peak-to-peak distances in the differential spectrum, we have to keep in mind mainly two factors: due to the background noise, the peak intensities are usually overestimated[10] and the intrinsic intensity for each Auger line depends on the element being analyzed. Luckily, the relative intensities are well-studied and transferrable onto other setups[3]. In general, the concentration information is only relative[1]. Strictly speaking, using the peak-to-peak distances requires the peaks in the integrated spectrum to be symmetric. Although this constraint is violated, we can assume the surface atoms to be either aluminium or oxygen in order to derive a rough but quantitative evaluation function for the cleaning process. This second assumption is justified, as the general overview spectrum in Figure 5 is dominated by oxygen and aluminium. The different sensitivity of the channeltron for different energies is of no importance in this case, as only the signal of electrons with a kinetic energy of less than 200 eV is significantly less amplified[3].

According to [3], the peak-to-peak distance δ_O for the oxygen peak at 510 eV is about 10.5 times the peak-to-peak distance δ_{Al} for the aluminium peak at 1396 eV. using the assumptions mentioned above, the relation

$$\delta_O = 10.5 \frac{c_O}{c_{Al}} \delta_{Al} \tag{6}$$

can be used to relate the two concentrations of aluminium and oxygen $c_i \in [0, 1]$. Now the surface coverage of aluminium is given by

$$c_{Al} = \left(1 + \frac{\delta_O}{10.5 \cdot \delta_{Al}}\right)^{-1} \tag{7}$$

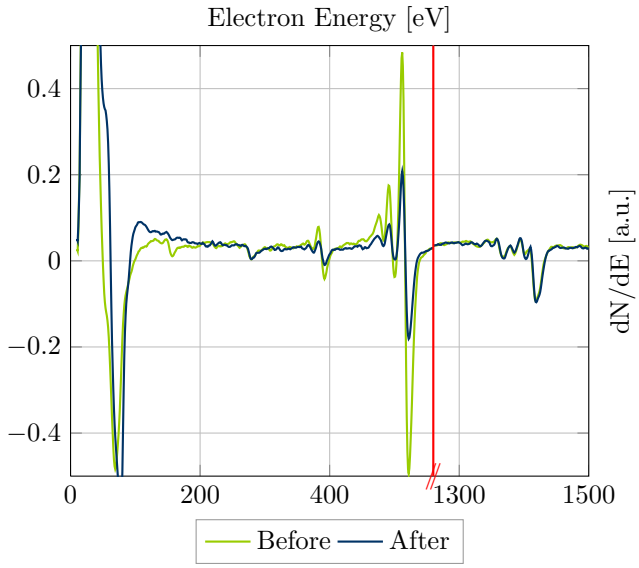

Figure 8. Measured Auger spectrum for the sample before and after the surface purification. The red line denotes a discontinuity, as the spectrum in-between is of lesser interest. Both spectra are averaged over three runs.

As Figure 8 shows, in the beginning δ_O/δ_{Al} is 7.6, thus the surface concentration of aluminium is about 58%. For reference, we estimated the concentration for the surface of pure aluminium after oxidation at standard conditions. The aluminium oxide layer is assumed to be much thicker than the mean depth of penetration[7]. That way, the usual Al_2O_3 molecular formula yields 40% aluminium coverage. As the pressure within the chamber is highly reduced, a significantly larger value for the sample used in this experiment is reasonable.

III.B Cleaned Sample

Figure 8 shows the differences between the initial spectrum and the spectrum after cleaning the sample surface. The estimated surface coverage for aluminium after the surface purification is about 78%. The penultimate evaluation run during the surface purification showed a spectrum matching a surface concentration for aluminium of about 87%. Unfortunately, during the last cleaning run, we lost this value. Maybe some remains on the file contaminated the sample again.

Figure 6 shows the Auger spectrum after the cleaning process. Most of the peaks are still observable and the positions of all these peaks reproduce the values from the uncleaned spectrum in Table IV. The sulfur peak has vanished and the $C^{(1)}$ peak is nearly completely covered by the $Al^{(1)}$ peak. Both the peaks for carbon and nitrogen are significantly smaller. The sizes of the oxygen peaks have been discussed already.

IV Plasmons

As the KLL part of the spectrum is mixed with plasmons[8], determining the plasmon energies helps telling the KLL lines and their plasmon deexitations apart. According to Figure 4, using primary electrons with a kinetic energy of 1 keV is more bulk sensitive, as the penetration depth is rather large when compared to primary electrons with a kinetic energy of 0.2 keV. However, the different energies only lead to tendencies, that is changing the peak heights. Both bulk and surface plasmons are expected to be detectable for both measurements.

IV.A Bulk Plasmons

After setting the primary electrons' kinetic energy to roughly 1 keV, we recorded the coarse differential spectrum from 10 eV to 1200 eV. Less surprisingly, we only found a minimal modulated peak for the reflected electrons. As the modulation is caused by the plasmons we like to analyze, we selected a smaller range of the spectrum and sampled with a resolution of 0.1 eV. Although the differentiated spectrum is rather clearly analyzable, [1] suggest using both the first and the second derivative of the $N(E)$ spectrum for determining the peak positions. By convention, we still use the high energy wing minimum of the first derivative as position of the peak. This position equals a change of sign for the second derivative. More specifically, the sign has to change from negative to positive. Due to the high inaccuracy of the primary electrons energy, which sums up to some 50-70 eV taking into account the offset shown in Table IV, only the energy losses compared to the highest peak are shown in Figure 9.

The peak position has been determined by searching for the zero crossings of the second derivative. The resulting positions and their interpretation is presented in Table V. Although the diagram shows even more bulk plasmons, the variation of the second derivative is in the magnitude of its noise. Therefore, we omitted the remaining peaks. The noise of the second derivative is mainly caused by the numerical accuracy of the first derivative which is discretized to units of 1/3 eV. Due to the energy sampling resolution of 0.1 eV, the error for the peak positions is at least 0.2 eV.

According to [1, 11], the spectrum may contain spurious peaks due to surface contamination. We attribute one peak to the adsorbate induced losses, as listed in Table V. As all of the peaks are clearly visible in the spectrum, we can make use of the fact that physically only integer numbers of plasmons are allowed. Therefore, the constant absolute error for the high loss plasmon peaks gives higher accuracy for a single plasmon excitation. Division by the number of bulk plasmons also reduces the absolute error for this measurement point. This method avoids doing a linear regression and thus, avoids introducing an axis intercept for the linear regression function

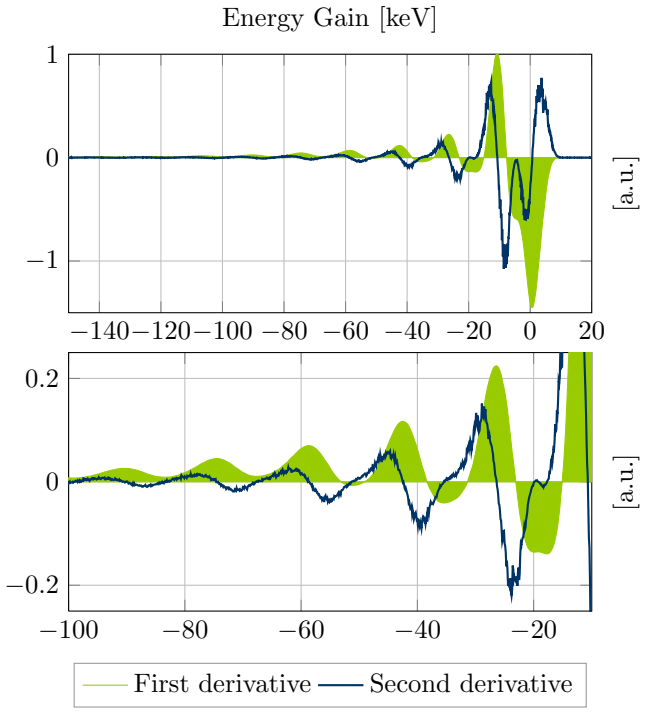

Figure 9. Measured EELS spectrum for aluminium at 1.0 keV (bulk sensitive). All datapoints are shifted to keep the highest peak at 0 eV. The first derivative data is drawn filled in order to allow for easy comparison. The second derivative is especially useful for resolving the double peak near -18 eV. The second derivative has been scaled by a factor of 2. Negative energy gain means energy loss. The first derivative was averaged over four independent spectra.

leading to systematically underestimated plasmon energies. Using the error weighted mean

$$E_B = \left(\frac{\sum_i E_i/(\Delta E_i)^2}{\sum_i 1/(\Delta E_i)^2} \pm \left[\sum_i 1/(\Delta E_i)^2 \right]^{-1/2} \right) \quad (8)$$

we get a bulk plasmon energy of

$$E_B = (16.75 \pm 0.03)\,\text{eV}$$

Table V. Measured peaks for the bulk plasmon EELS spectrum. All values in eV.

Energy	Loss	Interpretation
1065.7 ± 0.2	0	reference
1060.5 ± 0.2	4.5 ± 0.3	contamination
1047.3 ± 0.2	17.7 ± 0.3	bulk
1045.1 ± 0.2	19.9 ± 0.3	contamination and bulk
1029.6 ± 0.2	35.4 ± 0.3	two bulk plasmons
1013.7 ± 0.2	51.3 ± 0.3	three bulk plasmons
997.4 ± 0.2	67.7 ± 0.3	four bulk plasmons
981.5 ± 0.2	83.5 ± 0.3	five bulk plasmons
966.0 ± 0.2	99.0 ± 0.3	six bulk plasmons

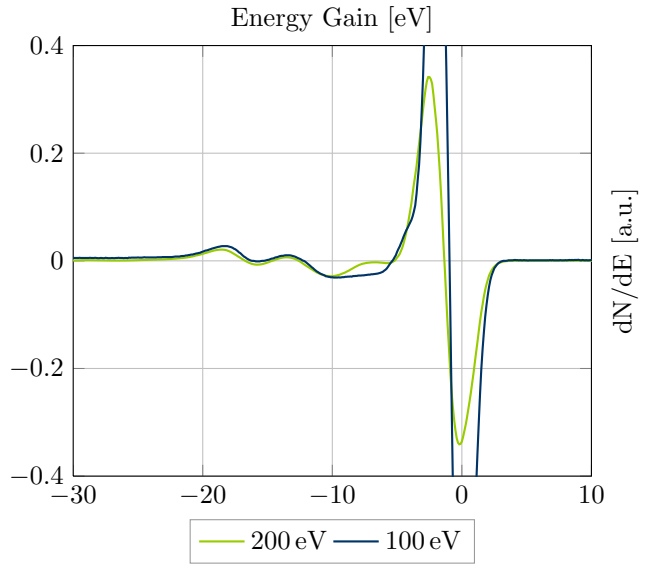

Figure 10. Measured EELS spectrum for aluminium at two different surface sensitive energies. All datapoints are shifted to keep the highest peak at 0 eV. Negative energy gain means energy loss. The first derivative was averaged over three independent spectra.

No surface plasmon excitations were observed in this spectrum. According to [8], the surface plasmons show only very small peaks that are possibly covered by others for this measurement. However, they are measurable even for a kinetic energy of 3.5 keV for the primary electrons[8].

IV.B Surface plasmons

In general, the analysis of this spectrum for 0.2 keV is the same procedure as in the last section. As no peaks next to each other were observed, the second derivative is omitted this time for the measured spectrum in Figure 10. The peaks and their interpretation are given in Table VI.

For the interpretation of the data, it was very helpful to know the energy of a bulk plasmon. As theory predicts a factor of $\sqrt{2}$ between the energy of the surface plasmon and the bulk plasmon for a sample in vacuum ($\varepsilon = 1$), we are precluded from assuming the contamination peak to

Table VI. Measured peaks for the surface plasmon EELS spectrum. All values in eV. All error values with an asterisk are estimated by the peak shape.

Energy	Loss	Interpretation
219.0 ± 0.2	0	reference
$213.5 \pm 0.3^*$	$5.5 \pm 0.4^*$	contamination
208.9 ± 0.2	10.1 ± 0.3	surface plasmon
203.3 ± 0.2	15.7 ± 0.3	bulk plasmon

be the first surface plasmon peak. We observed only one surface plasmon peak, hence no averaging is necessary. Our surface plasmon energy is

$$E_S = (10.1 \pm 0.3)\,\mathrm{eV}$$

This time, a surface plasmon loss peak could be observed. As theory predicts a better surface sensitivity for even lower primary electron energies, we set measured a spectrum with 0.1 kev, as shown in Figure 10. Instead of bigger peaks, we got less intense ones. This might be a result of the energy dependent gain for the electron multiplier, which drastically reduces the sensitivity for decreasing electron energies below 0.2 keV[3]. In case we would have any calibration data, we would be able to correct the spectrum according to the gain profile. For even lower energies, 60 eV, no plasmon peaks could be observed.

IV.C KLL Transitions

Now that we know the plasmon energies, we can search for the KLL peaks in the Auger spectrum in Figure 11. The found peaks are given in Table VII. As the reference data is given with respect to the Fermi energy level, the work function has to be taken into consideration for absolute values. Due to the offset to be discussed later on, it is more precise to look at the energy shifts from Table VII for the quantitative comparison with reference data[8]. For all KLL transitions with the exception of KL_1L_1, the measured shifts are statistically equal to the reference data. For the KL_1L_1 transition, the values are compatible. The $KL_{2,3}L_{2,3}$ (^{3}P) transition forbidden by LS coupling[8] could not be observed.

V Discussion

V.A Offset

Estimating the work function to 4 eV, the absolute energies of the reference data[8] for the KLL transitions can be related to the measured values. Combining this information with the offset from the peaks in Table IV, we can

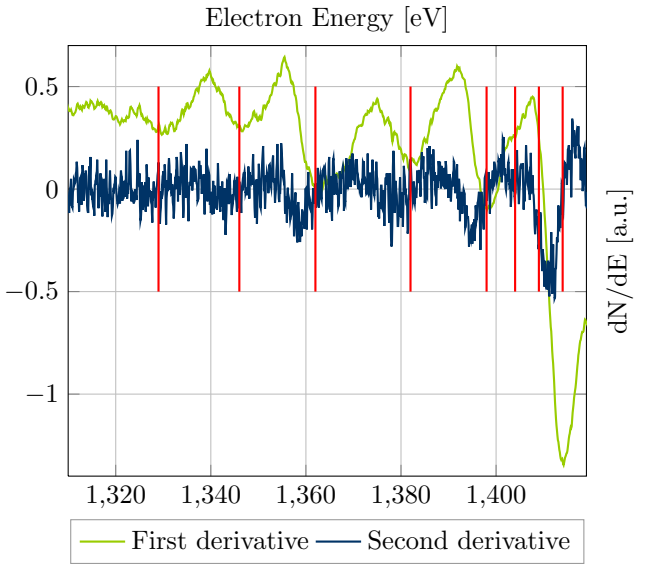

Figure 11. Measured Auger KLL spectrum for aluminium. All peaks are marked with red lines and explained in Table VII. Only the first derivative was measured, the second one was computed from the measured data, hence the rather high noise level.

show the dependency of the apparent offset on the absolute energy. The data in Figure 12 shows a nearly linear behaviour suggesting a systematic scaling error. However, this scaling error is quite small and can be found by linear regression

$$\Delta E = 0.012E + 3.7\,\mathrm{eV}$$

The coefficient of determination is 0.91. Using this relation, we can correct the measured values from Table VII by this offset in order to compare the absolute values to the reference. The results for the KLL transitions are given in Table VIII. That way, all absolute values are statistically equal to the reference values.

V.B Plasmon and KLL Energies

The energy for the surface plasmons are statistically equal to the reference values[8], whereas the results for the bulk plasmons show a significant difference. As not

Table VII. Measured peaks for the KLL Auger spectrum. All values in eV. The shift is calculated with reference to the $KL_{2,3}L_{2,3}$ (^{1}D) line.

energy	shift	interpretation
1414 ± 1	0	$KL_{2,3}L_{2,3}$ (^{1}D)
1409 ± 1	-5 ± 3	KL_2L_3 (^{1}S)
1404 ± 1	-10 ± 3	surface plasmon (weak)
1398 ± 1	-16 ± 3	bulk plasmon
1382 ± 1	-32 ± 3	$KL_1L_{2,3}$ (^{3}P)
1362 ± 1	-52 ± 3	$KL_1L_{2,3}$ (^{1}P)
1346 ± 1	-68 ± 3	four bulk plasmons
1329 ± 1	-85 ± 3	KL_1L_1 (^{1}S)

Table VIII. Measured peaks for the KLL Auger spectrum. All values in eV. For the correction method, see text. All energies in eV.

corrected	reference	interpretation
1390 ± 2	1393.5 ± 0.2	$KL_{2,3}L_{2,3}$ (^{1}D)
1385 ± 2	1386.6 ± 0.2	KL_2L_3 (^{1}S)
1358 ± 2	1358.5 ± 0.2	$KL_1L_{2,3}$ (^{3}P)
1338 ± 2	1342.3 ± 0.2	$KL_1L_{2,3}$ (^{1}P)
1306 ± 2	1304.0 ± 0.2	KL_1L_1 (^{1}S)

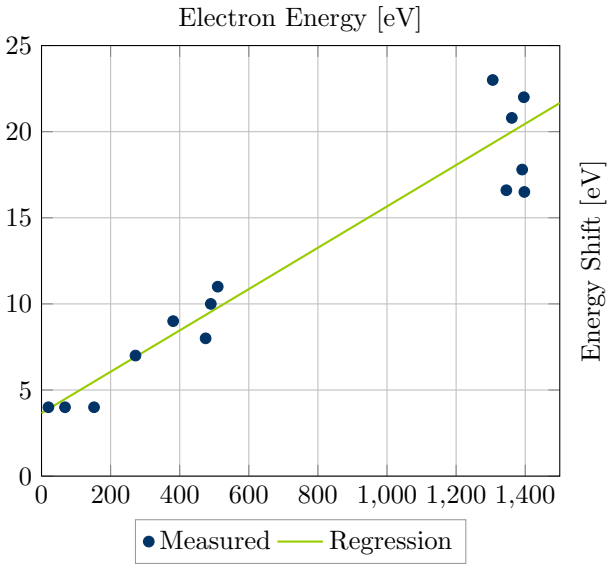

Figure 12. Dependency of the offset for measured energies on the absolute energy when compared to reference data.

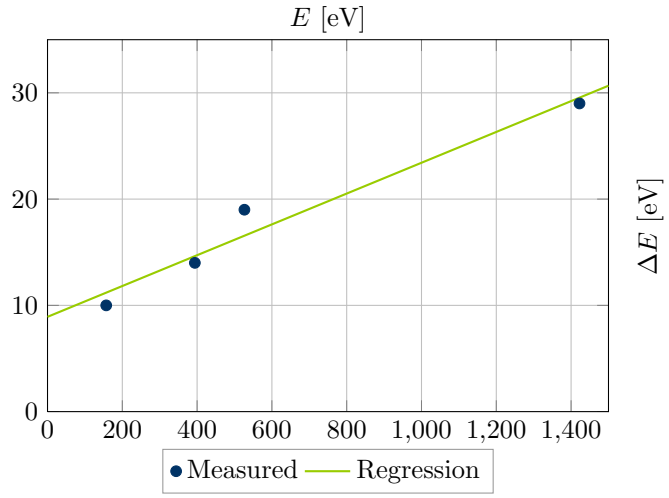

Figure 13. Dependency of the peak width on the absolute energy in order to confirm constant resolution.

even the relative factor between E_S and E_B matches the theoretical values, it is most likely an error in the measurement of E_B.

However, the theoretical factor of $\sqrt{2}$ does not even hold for the reference data. Applying this factor to the reference E_S would give an barely compatible value for the reference E_B. Therefore, the tendency to a higher factor between E_S and E_B than $\sqrt{2}$ can be confirmed. As the contamination peak in Table V is rather intense, one may suspect the surface adsorbate to influence the secondary electrons of the AUGER process even for bulk plasmon excitation.

Certainly, the effect would have to be the same for the surface plasmons. As their value is less than the reference data but the bulk plasmons' value is larger than the reference, we discarded this idea. The effect of the remaining gases in the vacuum chamber is neglectable, as well. For low pressures, ε depends logarithmically[12] on pressure and reaches 1 for vacuum. Hence, the energy factor $\sqrt{1+\varepsilon}$ remains mostly unaffected for small pressure differences. The error is more likely to be caused by the overlap of several peaks. To overcome this limitation, an even higher resolution would be necessary.

One has to keep in mind, that resolution is meant to be $\Delta E/E$ not the sampling rate. The resolution of a cylindrical mirror analyser is expected to be constant[1]. Figure 13 shows the dependency of the peak width on the absolute energy for the aluminium, oxygen, nitrogen and sulfur peak from Figure 5 and confirms this expectation.

The reference energies are fully reproduced for all expected KLL peaks.

[1] G. Ertl, *Low Energy Electrons and Surface Chemistry* (Wiley VCH, 1985).
[2] S. Hofmann, *Auger- and X-Ray Photoelectron Spectroscopy in Materials Science* (Springer, 2012).
[3] L. E. Davis, *Handbook of Auger Electron Spectroscopy* (Eden Prairie, 1972).
[4] W. Demtröder, *Experimentalphysik 3* (Springer, 2010).
[5] S. Hofmann, *Moderne Physik* (Springer, 2012).
[6] J. Riviere, *Handbook of Surface and Interface Analysis: Methods for Problem-Solving* (CRC Press, 2009).
[7] K. Iakoubovskii, K. Mitsuishi, Y. Nakayama, and K. Furuya, Phys. Rev. B **77**, 104102 (2008).
[8] G. Dufour, J.-M. Mariot, P.-E. Nilsson-Jatko, and R. C. Karnatak, Physica Scripta **13**, 370 (1976).
[9] P. Haudrechy, B. Mantout, A. Frappaz, D. Rousseau, G. Chabeau, M. Faure, and A. Claudy, Contact Dermatitis **37**, 113 (1997).
[10] J. M. Walls, *Methods of Surface Analysis: Techniques and Applications* (Cambridge University Press, 1989).
[11] D. Massignon, F. Pellerin, J. M. Fontaine, C. L. Gressus, and T. Ichinokawa, Journal of Applied Physics **51**, 808 (1980).
[12] J. F. Skinner, E. L. Cussler, and R. M. Fuoss, The Journal of Physical Chemistry **72**, 1057 (1968).